Iron Deposition and Ferroptosis in the Spleen in a Murine Model of Acute Radiation Syndrome

William B. Rittase
Uniformed Services University of the Health Sciences
John E. Slaven
Uniformed Services University of the Health Sciences
Jeannie M. Muir
Uniformed Services University of the Health Sciences
Sang-Ho Lee
Uniformed Services University of the Health Sciences
Milan Rusnak
Uniformed Services University of the Health Sciences
Grace V. Brehm
Uniformed Services University of the Health Sciences
Aviva Symes
Uniformed Services University of the Health Sciences
Regina M. Day (regina.day@usuhs.edu)
Uniformed Services University of the Health Sciences

Research Article

Keywords: Total body radiation (TBI), death , hematopoietic insufficiency, Iron Deposition, Ferroptosis

Posted Date: November 10th, 2021

DOI: https://doi.org/10.21203/rs.3.rs-1031783/v1

Abstract

Total body radiation (TBI) can result in death associated with hematopoietic insufficiency. Although radiation causes apoptosis of white blood cells, red blood cells (RBC) undergo hemolysis due to hemoglobin denaturation. RBC lysis post-irradiation results in the release of iron into the plasma, producing a secondary toxic event. We investigated the impact of radiation-induced iron release on the spleen of mice following TBI and the effects of the radiation mitigator captopril. RBC and hematocrit were reduced ~7 days (nadir ~14 days) post-TBI. Prussian blue staining revealed ~20-60-fold increased Fe3+ in the spleen 7-14 days post-irradiation, also associated with altered expression of iron binding and transport proteins, determined by qPCR, western blotting, and immunohistochemistry. Captopril did not prevent iron deposition in the spleen, and did not significantly modulate most iron-binding proteins. Spleen volumes were markedly decreased 7-14 days, correlating with high Fe3+. At these time points, caspase-3 was activated and we identified four markers of ferroptosis, iron-dependent programmed cell death. Interestingly, p21/Waf1, a marker of accelerated senescence, was not upregulated in vivo. Macrophage inflammation is an important effect of TBI. We investigated the effects of radiation and Fe3+ on the cultured J774A.1 murine macrophage cell line. Radiation induced p21/Waf1 and ferritin, but not caspase-3, within 24 h. Radiation ± iron upregulated several markers of pro-inflammatory M1 polarization; radiation with iron also upregulated a marker of anti-inflammatory M2 polarization. Our data indicate that following TBI, iron accumulates in the spleen where it regulates iron binding proteins and triggers ferroptosis.

Introduction

The hematopoietic system is markedly sensitive to damage by radiation [1]. In humans, exposure to 4-6 Gy of total body irradiation (TBI) can lead to the development of hematopoietic subsyndrome of acute radiation syndrome (H-ARS), characterized by hematopoietic insufficiency, opportunistic infection from immune suppression, acute inflammatory response, and coagulation dysfunction [1-5]. Mature white blood cells (WBC) and many hematopoietic progenitors undergo apoptosis following exposure to high dose radiation [5,6]. Reticulocytes and red blood cells (RBC) lack DNA and apoptotic machinery and instead undergo hemolysis driven by the oxidation and denaturation of hemoglobin (HGB) [5,7,8]. Apoptosis of mature WBC contributes to immune insufficiency and opportunistic infection [9], while the destruction of RBC contributes to poor oxygenation and the potentially toxic release of iron [10,11].

Iron is a nutritionally essential element, required for many basic biological activities, including the generation of ATP by mitochondrial respiration and oxygen transport [12]. The conversion of iron between the ferric (Fe^{3+}) and ferrous (Fe^{2+}) states allows single electron transfers, a process required in a variety of biochemical reactions [12]. However, excessive iron is associated with biologically toxic effects. Free iron can promote the generation of toxic free radicals resulting from its interaction with oxygen, as described in the Fenton and Haber-Weiss reactions [13,14]. Dysregulated iron accumulation in a variety of tissues and

iron-catalyzed free radicals have been proposed to play a role in cancer, metabolic diseases, blood disorders, and multiple degenerative diseases [14-16].

Proteins involved in the binding and transport of iron are highly conserved in mammals [17]. Additionally, the processes for iron handling, from absorption in the intestine to transport in the plasma and storage in the liver, are tightly regulated and highly conserved evolutionarily [17-21]. Erythropoiesis accounts for the most abundant usage of iron, and 65-75% of the total iron in mammals is bound to hemoglobin within erythrocytes [17]. Homeostatic iron recycling occurs within the spleen, where RBC are removed from circulation based on abnormal size, shape, or deformability as well as markers for senescence [22]. Effete or damaged RBC, detected within the spleen, undergo erythrophagocytosis by specialized red pulp macrophages [23,24]. In other tissues, macrophages provide iron homeostasis by sensing and responding to microenvironmental iron concentrations [25]. Although specialized macrophages normally take up iron for recycling, high levels of iron within macrophages can affect their function. Iron accumulation in macrophages is associated with the suppression of pro-inflammatory M1-like polarization and increased anti-inflammatory, M2-like polarization [25].

Our laboratory and others have demonstrated that radiation-induced hemolysis of RBC is associated with an accumulation of iron in the bone marrow in rodent models of H-ARS [26,27]. Here we investigated the deposition of iron in the spleen following TBI in mice. We found that Fe^{3+} iron accumulation in the spleen was maximal ~14 days post-irradiation, correlating with the maximal loss of RBC and hematocrit (HCT) after TBI. Increased iron in the splenic tissue was associated with increased levels of iron binding and transport proteins. Interestingly, increased iron in the spleen was associated with increased activation of caspase-3, a regulator of programmed cell death. Further investigation revealed the simultaneous regulation of a number of markers for ferroptosis, an iron-dependent form of programmed cell death. Histological analysis indicated that iron storage and expression of iron storage proteins within the spleen occurred mostly within splenic macrophages. Because iron and radiation are known to affect polarization of macrophages, we investigated the effects of iron, radiation, and iron + radiation on M1 and M2 polarization of J774A.1 murine macrophages in culture. Exposure to radiation induced accelerated senescence. Radiation and radiation + iron resulted in the upregulation of markers of M1. Radiation + iron moderately upregulated one marker of M2 polarization in the cultured macrophages. These data provide evidence for Fe^{3+} release as a secondary toxic event following exposure to total body ionizing radiation. Additionally, the presence of Fe^{3+} following radiation exposure in vivo may play a role in pro-inflammatory responses after TBI.

Results

Sub-lethal irradiation reduces red blood cells, hematocrit, and hemoglobin

Female C57Bl/6J mice were exposed to 6.85 Gy TBI (0.6 Gy/min). This sublethal dose of radiation did not result in mortality in any groups. Previous studies showed that radiation induces the hemolysis of RBC and reticulocytes due to the denaturation of hemoglobin [8,10]. 6.85 Gy irradiation caused a significant reduction in RBCs, HCT, and HGB, with maximal ~60% reduction around day 14 (Fig. 1A-C). Because this sublethal radiation exposure dose causes only a relatively low level of blood cell reduction, no significant differences were observed between vehicle- and captopril-treated animals (Fig. 1A-C). The mean corpuscular volume (MCV), an indicator of the average erythrocyte size, was near baseline for days 7 and 14 post-irradiation in both vehicle and captopril groups (Fig. 1D). MCV exceeded the normal volumes on day 21 in vehicle-treated animals, but not in the captopril-treated group (Fig. 1D). Interestingly, the mean corpuscular HGB concentrations (MCHC) were maintained in captopril-treated mice over the full duration of the time course, while in vehicle-treated animals, the MCHC fell below basal levels at day 21 post-irradiation (Fig. 1E). Together, these data show that in the vehicle-treated group there is increased level of reticulocytes as indicated by the higher MCV along with corresponding lower mean concentration of hemoglobin per cell volume at 21 days. This represents an erythropoietic response to the loss of erythrocytes, with the loss most pronounced at 14-days. The increase in the circulating reticulocytes is further supported by the decreased MCHC in an inverse fashion compared to the change in the MCV. However, this increase is minimal in the case of captopril-treated group that has more gradual erythropoietic recovery. Overall there is an erythropoietic response most noticeable on day 21 for vehicle-treated group as indicated by the maximum MCV reflecting the robust release of immature erythrocytes from the bone marrow in the forms of larger reticulocytes to compensate the radiation-induced loss of erythrocytes.

Sub-lethal irradiation results in iron deposition in the spleen and upregulation of genes encoding iron handling proteins

Our laboratory and others demonstrated that following radiation-induced hemolysis, iron is deposited within the bone marrow [27,28]. Iron recycling normally occurs within the spleen, where specialized macrophages take up senescent or damaged RBC [24]. We therefore investigated spleen iron levels following TBI. Within 7-14 days, Prussian blue staining, that detects Fe^{3+}, increased ~20-60-fold (Fig. 2A, B). Prussian blue staining returned to near basal levels by day 21. Histological analysis revealed that granular staining was primarily cytoplasmic within splenic histiocytes/macrophages. Captopril treatment did not significantly affect iron deposition in the spleen (Fig 2B).

We examined gene expression of iron binding and transport proteins following exposure to TBI (Fig. 3). Three patterns of gene expression changes were evident in the data. In the first group, *Fth1* (ferritin heavy chain), *Slc40a1* (ferroportin), and *Trf* (transferrin) were significantly upregulated at 7 days, with declining expression to near basal levels at 14-28 days post-irradiation (Fig. 3A-C). Ferritin heavy chain is associated with storage, primarily within macrophages. Iron is exported by cells through the transporter ferroportin that passes iron to transferrin, the primary protein for secure transport of iron through the

plasma [23]. The second group, *Tfrc* (CD71/ transferrin receptor), *Itgam* (integrin alphaM, also known as Mac-1 or CD11b/CD18), and *Lcn2* (lipocalin-2) exhibited initial suppression followed by increased expression ~14-21 days (Fig. 3D-F). The CD71/transferrin receptor binds transferrin from the plasma for import of iron into the cell, while integrin alphaM has been shown to bind to and import iron oxide nanoparticles [29,30]. Lipocalin-2 binds iron for uptake into cells where it can be sequestered [31-33]. Finally, we examined expression of *Flvcr1* which encodes two heme export proteins important for cellular heme homeostasis: feline leukemia virus subgroup C receptor 1a (FLVCR1a) a plasma membrane heme exporter, and FLVCR1b, a mitochondrial protein [34,35]. *Flvcr1* displayed reduced expression (~50%) at 28 days in vehicle-treated animals (Fig. 3G), suggesting a reduction in the uptake of heme-bound iron. Captopril treatment did not alter the expression of most of these genes. Captopril did enhance the expression of integrin alphaM at 21 days, with a trend toward increased expression at 28 days. Captopril also significantly enhanced the expression of lipocalin-2 at 21 and 28 days (Fig. 3E, F).

Immunohistochemistry (IHC) was used to identify cell types expressing several of the iron handling genes. As described above, ferritin gene expression increased ~7 days (Fig 4A, B). IHC showed a trend toward increased ferritin expression in the spleen at 7 days, declining at 14 and 21 days. Ferritin staining in irradiated spleens was granular in appearance and localized to the cytoplasm and dendritic processes of histiocytes/macrophages, with especially strong staining in cells in the sinuses under the spleen capsule (Fig. 4A). Western blotting showed significant increases in ferritin (~5-6-fold, $p<0.05$) at 7-14 days (Fig. 4C). Hemosiderin, an iron storage complex containing ferritin and Fe^{3+}, appeared as gold-brown coloration (Fig. 4D). Data show that there was a significant increase in hemosiderin at 7-14 days (~4-fold higher than control, $p<0.05$), and 28 days (~2-fold higher than control, $p<0.05$).

qPCR showed an increase in the CD71/transferrin receptor, ~14-21 days post-irradiation. IHC showed a trend toward increased CD71 levels (~2-fold) 21 days post-irradiation (Fig. 5A, B). CD71 staining was prominent in red pulp, localized to the cytoplasmic membranes of erythrocytes, including nucleated immature erythrocytes. Staining was not identified within histiocytes/macrophages. Western blotting confirmed ~40-fold upregulation of ferritin at 7-14 days ($p<0.05$) (Fig. 5C). IHC was used to examine levels of CD163, a high affinity scavenger receptor for the hemoglobin-haptoglobin complex [36](Fig. 6A, B). CD163 levels were suppressed at all time points, to ~1/3 control levels. Staining was mostly present in the control samples, localized to the cytoplasm of histiocytes/macrophages of in the red pulp in the same cells that were stained with Prussian blue.

Reduction in spleen volume post-irradiation is associated with ferroptosis.

Our laboratory previously showed that the size of the spleen is reduced ~10 days following TBI in mice [37]. We investigated the effect of radiation on the spleen weight, normalized to total body weight (Fig. 7A). The normalized spleen mass is reduced to ~50% of control ($p<0.05$) at 7 and 14 days post-irradiation in

both vehicle and captopril treated animals, correlating with the times of highest levels of iron deposition in the spleen. Western blotting for upregulation of activated caspase 3 as a marker of programmed cell death revealed a significant increase in proteolytic fragments at 7 and 14 days post-irradiation in vehicle-treated mice (Fig. 7B, left panel; $p<0.05$). In captopril-treated animals, caspase 3 activation was also increased, significant at 14 days post-irradiation (Fig. 7B, right panel; $p<0.05$) Interestingly, we did not observe increased expression of p21/Waf1, a marker of cell cycle inhibition and accelerated senescence (Fig. S1).

Recent studies showed that high levels of iron can induce ferroptosis, a form of programmed cell death [38,39]. Ferroptosis markers include increased expression of CD71/ferritin receptor 1, and reduced glutathione peroxidase 4 (GPX4) and solute carrier family 7 member 11 (Slc7A11) [38,40]. We demonstrated increased expression of the CD71 using qPCR (Fig. 3) and western blotting (Fig. 5B); IHC of the spleen showed that this increase occurred within mature and immature erythrocytes. We next investigated the gene expression of *Gpx4* and *Slc7a11* in the total spleen tissue (Fig. 7C,D). *Gpx4* expression showed a trend toward decreased expression (~25% reduced) within 7 days post-irradiation, and was significantly suppressed, to less than 50% basal levels, at 14 and 21 days post-irradiation ($p<0.001$-0.0001) compared with basal levels. In vehicle-treated animals *Gpx4* returned to near basal levels at 28 days post-irradiation; captopril treatment resulted in *Gpx4* remaining significantly lower than basal levels at 28 days ($p<0.05$). In contrast, *Slc7a11* showed a slight trend toward increased expression at 7 days post-irradiation, followed by a trend toward reduced expression at 14 days post-irradiation in both vehicle- and captopril-treated groups. *Slc7a11* was significantly reduced only in vehicle-treated animals at 21 days post-irradiation ($p<0.0001$). In captopril-treated animals, *Slc7a11* remained near basal levels over the time course.

Cyclooxygenase-2 (COX-2) is also marker, but not a driver, of ferroptosis [38]. Western blotting showed that COX-2 protein levels were significantly increased at 7 days post-irradiation in vehicle-treated animals (Fig. 7E, left panel; $p<0.05$). We observed a trend toward increased COX-2 protein in captopril-treated animals, but this did not reach significance (Fig. 7E, right panel).

Iron- and radiation-induced alterations in gene expression in culture murine macrophages.

Macrophages play a key role in iron homeostasis as well as in normal immune responses [23]. Iron regulates iron binding and transport proteins in macrophages and modulates macrophage polarity [17,41,42]. Iron exposure upregulates ferritin and several other iron storage and transport proteins in macrophages [17], and impairs the ability of macrophages to assume a full pro-inflammatory (M1) phenotype [41]. However, *in vitro* studies showed that radiation had no effects on macrophage polarity [43]. In contrast with *in vitro* studies, *in vivo* studies of TBI have shown effects on macrophage polarization,

favoring the induction of M1 polarization early after radiation, followed by the development of alternatively activated (anti-inflammatory or M2) macrophages [44,45].

Because the *in vivo* effects of total body radiation likely reflect the impact of radiation with iron on macrophages, we wished to determine the effects of iron, radiation, and iron + radiation on macrophage polarization *in vitro*. We utilized 7 and 12.5 mg/L Fe^{3+} in the medium based on reported iron concentrations in the serum following TBI in mice [10]; iron was combined with two doses of radiation that are sublethal when used in TBI studies in C57BL/6 mice [46]. We examined the gene expression of three markers of pro-inflammatory M1 polarization, inducible nitric oxide synthase (iNOS), interleukin-6 (IL-6) and IL-1β (Fig. 8A-C). Of these, radiation significantly induced *Nos2* and *Il1b*, but not *Il6*. Iron alone did not activate any markers of M1 polarity, but the presence of iron in the medium did show a trend toward augmenting iNOS expression (Fig. 8A). Neither iron alone nor radiation alone activated the M2 marker *Arg1* (arginase 1) (Fig. 8D). Iron + radiation did result in the upregulation of *Arg1*, although not consistent for all radiation + iron conditions (Fig. 8D). We next examined the ability of M1- or M2-inducing cytokines (IFN-γ + LPS for M1; IL-4 for M2) to induce polarization in the presence of iron, radiation, or iron + radiation (Fig. 9). Iron, radiation, or iron + radiation did not inhibit the upregulation of *Il6* or *Il1b* induction by IFN-γ + LPS or *Arg1* induction by IL-4. Together, these data suggest that radiation and iron + radiation may induce mixed polarity but they do completely block cytokine responses by the macrophages.

Our *in vivo* data indicated that macrophages in the spleen contain high levels of ferritin after TBI. To determine the effects of high iron concentrations and ionizing radiation on iron binding protein expression, we examined the levels ferritin in J774A.1 cultured macrophages. We found ~6-14 fold upregulation of ferritin heavy chain in all cultures that included high iron within 24 h ($p<0.05$, Fig. 10A). Interestingly, upregulation of ferritin heavy chain protein was not significantly affected by radiation exposure or by M1- or M2-inducing cytokines, although radiation and M1-inducing cytokines did upregulate gene expression of *Fth* at 24 h (Fig. S2). We did not detect significant levels of transferrin receptor 1 in the cultured macrophages before or after irradiation.

In vivo data also indicated that significant levels of programmed cell death, but not accelerated senescence, occurred in the spleen following TBI. However, our previous studies indicated that ionizing radiation induces accelerated senescence in cultured pulmonary artery endothelial cells [47]. The spleen contains significant levels of macrophages as well as microvascular endothelial cells. We investigated programmed cell death and senescence in cultured J774A.1 and human spleen microvascular endothelial cells. J774A.1 cells displayed a trend toward increase in p21/waf1, a marker for accelerated senescence, after exposure to 2 or 6.85 Gy ionizing radiation (Fig. 10B). Senescence was significant in 6.85 Gy irradiated cells in the presence of iron (Fig. 10B). Neither iron alone nor M1- or M2-inducing cytokines induced p21/waf1. We did not detect significant caspase-3 activation under any conditions (data not shown). Because the spleen contains a fairly large population of microvascular endothelial cells, we investigated the effects of radiation and high iron exposure on human spleen microvascular endothelial cells (HSpMVEC) in culture. Interestingly, we were unable to detect either caspase-3 activation or

p21/waf1 upregulation in HSpMVEC at 24 h following radiation, iron, or iron + radiation exposure (Fig. S3).

Discussion

Exposure to total body ionizing radiation can result in H-ARS, characterized by hematopoietic insufficiency, immune suppression, opportunistic infection, and coagulopathy. The acute effects of radiation have been extensively studied *in vivo* and *in vitro*, but the etiology of some of the chronic effects of radiation (weeks or months after initial exposure) are not well understood. Here we demonstrate that exposure to sublethal TBI results in the loss of RBC and HGB, allowing release of iron that can be sequestered within the spleen, detected as Fe^{3+} complexes. Our data indicate that deposition of iron in the spleen is correlated with the regulation of iron binding and transport proteins and with ferroptosis. This suggests that iron, released from radiation-induced hemolysis, acts as a toxic agent following exposure to even sublethal levels of ionizing radiation.

Our data indicated that there are at least three phases of regulation of iron binding and transport proteins following TBI. In the first phase, ferritin heavy chain, transferrin, and ferroportin were increased at 7 days post-irradiation and fell to near basal levels thereafter. Ferritin heavy chain is the primary storage complex for Fe^{3+} iron within macrophages while transferrin is the primary protein for the secure transport of Fe^{3+} through the plasma [23]. The transporter ferroportin passes Fe^{3+} iron from the cellular cytoplasm to transferrin. The increased expression of these three proteins at 7 days suggests an early transient phase of increased iron storage in ferritin and iron packaging into transferrin. In the second phase of regulation, we observed upregulation of CD71/transferrin receptor, integrin alphaM/Mac-1, and lipocalin-2 between 7-14 days. These remained elevated over the time course, except for CD71/transferrin receptor, which returned to basal levels. The CD71/transferrin receptor binds transferrin from the plasma for import into the cell, while integrin alphaM has been shown to bind to and import iron oxide nanoparticles [29,30]. Lipocalin-2 participates in the regulation of iron homeostasis [32,33] and safely sequesters and transports iron [31,32]. These data suggests a secondary phase of uptake of transferrin, regulation of iron homeostasis, and possibly uptake of iron particles. Finally, in the third pattern of expression, we observed suppression of *Flvcr1* gene expression and CD163 over the time course of the experiment. FLVCR1a functions to export heme-bound iron from macrophages and other cell types [34]. In contrast, CD163 is a high affinity scavenger receptor for the hemoglobin-haptoglobin complex [36]. Together, these data suggest that following radiation-induced hemolysis, there is a suppression of proteins required for the transport of heme iron complex but biphasic upregulation of other iron binding and transport proteins. The mechanisms that regulate the timing of these events following radiation are not known.

We found that the presence of high levels of iron in the spleen correlate with the activation of programmed cell death, as indicated by caspase-3 activation, primarily on days 7-14. We also identified the alteration of four markers of ferroptosis, including upregulation of ferritin receptor and COX-2, and downregulation of GPX-4 and SLC7A11. The significance of increased ferritin receptor expression is that

this receptor is believed to provide transport of iron into the cell, where it may then cause the generation of reactive oxygen species (ROS) at toxic levels if it is not efficiently sequestered. The GPX-4/SLC7A11 proteins provide a mechanism of protection against iron-induced ROS, by detoxification; downregulation of these proteins is consistent with the lack of antioxidant protective response within the cell. COX-2 protein has been shown to be a marker, but not driver, of ferroptosis. Histological analysis for the cellular expression of the ferritin receptor suggested that this receptor is increased on reticulocytes and reticulocyte precursors. Further investigation is needed to determine the cell types that undergo ferroptosis in the spleen following TBI as well as ferroptosis in other tissues.

Iron and radiation have both been shown to modulate macrophage polarity [23,34,43]. Our data suggest that TBI would necessarily result in both radiation damage to macrophages and their exposure to high levels of iron. Our cell culture murine macrophage studies indicate that iron alone does not significantly upregulate the pro-inflammatory M1 polarization markers tested, whereas radiation exposure and iron + radiation can upregulate iNOS and IL-1β. Arg-1, an anti-inflammatory M2 polarization marker, can be upregulated by combined radiation + iron. Neither iron, radiation, nor the combination inhibited cytokine-induced M1 or M2 polarization. While our investigation of macrophage polarization is not exhaustive, our data suggest that combined iron + radiation may induce a mixed polarity. This issue also merits further exploration, especially given the importance of delayed inflammation following radiation exposure.

Previous studies from our laboratory have shown that captopril mitigates ARS in mice and in Göttingen minipigs [27,46]. However, our current data indicate that captopril treatment did not mitigate radiation-induced reduction of RBC or HGB, or deposition of iron in the spleen. Consistent with this, captopril did not modulate most of the expression of iron binding or iron storage proteins, and did not significantly suppress ferroptosis. Captopril treatment enhanced integrin alphaM and lipocalin-2 post-irradiation. Because integrin alphaM is also macrophage marker, this could indicate improved recovery of macrophages or improved iron homeostasis.

In summary, our findings indicate that the spleen is a major organ for the deposition of iron following hemolysis after exposure to ionizing radiation, resulting in ferroptosis in the spleen. Additionally, iron and radiation together may affect the polarization of tissue macrophages, potentially inducing mixed polarity. Improved understanding of the effects of iron as a secondary toxicity following TBI may allow for advancements in the treatment of delayed radiation tissue damage.

Methods

Chemicals:

Reagents were obtained from Millipore Sigma (St. Louis, MO, USA) except where indicated.

Animals and captopril treatment:

All animal handling procedures were performed in compliance with guidelines from the National Research Council for the ethical handling of laboratory animals and were approved by the Uniformed Serviced University of Health Sciences (USUHS) Animal Care and Use Committee (Protocol PHA-20-025). ARRIVE guidelines were also followed for the use of animals in this study. Female C57BL/6J mice were purchased from Jackson Laboratories (Bar Harbor, ME, USA). Mice were kept in a barrier facility for animals accredited by the Association for Assessment and Accreditation of Laboratory Animal Care International. Mice were housed in groups of four. Animal rooms were maintained at 21 ± 2°C, 50% ± 10% humidity, and 12 h light/dark cycle with freely available rodent ration (Harlan Teklad Rodent Diet 8604, Frederick, MD, USA). Animals were randomized to treatment groups for each experiment, using the appropriate numbers of animals to ensure significance. At 12-14 weeks of age, mice were placed in Lucite jigs and exposed to TBI in a bilateral gamma radiation field in the Armed Forces Radiobiology Research Institute (AFRRI, Bethesda, MD, USA) high level ^{60}Co facility as previously described [48]. The midline tissue dose to the mice was 6.85 Gy at a dose rate of 0.6 Gy/min, a sub-lethal radiation exposure for this strain of mice. The alanine/electron spin resonance (ESR) dosimetry system was used to measure dose rates (to water) in the cores of acrylic mouse phantoms [49]. Sham irradiated control groups were placed in Lucite jigs but without exposure to radiation. Captopril (USP grade; MilliporeSigma) was dissolved at 0.13 g/L in acidified water [50] to deliver ~13-26 mg/kg/day [46,51]. Captopril in the water was provided to animals from 2 days post-irradiation for 14 consecutive days [46,51]. Control animals received acidified water (vehicle) without captopril. All animals in this study also received injections of saline (100 µl subcutaneously) on the same days as captopril administration, as these groups were control groups from another study. Euthanasia was performed by injection of 0.1-0.2 ml Fatal Plus (Vortech Pharmaceuticals, Dearborn, MI, USA; 39-78 mg pentobarbital) per animal in accordance with current American Veterinary Medical Association Guidelines for Euthanasia. Euthanasia was ensured prior to collection of tissues.

Histology and immunohistochemistry (IHC):

Spleens were surgically removed from euthanized animals and fixed in 10% neutral buffered formalin overnight. Tissues were processed and embedded in paraffin using standard methods and stained for hematoxylin and eosin (H&E) and Prussian blue staining (Histoserv, Inc., Germantown, MD, USA). For immunohistochemistry (IHC), antigen retrieval was performed on paraffin-embedded sections prior to blocking and incubation with primary and secondary antibodies. Details for IHC are provided in Supplemental Section. Spleen sections were digitally scanned using the Ziess Axioscan for analysis and images for publication were produced with Zen Lite software (Carl Ziess Meditech, Inc., Dublin, CA, USA). Stained slides were evaluated by a pathologist who was blinded to the identity of the treatment groups.

Cell culture, irradiation, and iron treatment:

The J774A.1 murine macrophage cells (American Tissue Culture Collection, Manasses, VA, USA) were cultured in Dulbecco's Modified Eagles Medium (Quality Biological, Gaithersburg, MD, USA; Catalog #:112-

300-101), 10% fetal bovine serum (Gemini Bio, West Sacremento, CA, USA), with penicillin (100 units/ml) and streptomycin (100 µg/ml), 0.5% fungizone (Gibco/ThermoFisher Scientific, Waltham, MA, USA). Primary human spleen microvascular endothelial cells (HSpMVEC; Cell Biologics, Chicago, IL, USA) were grown in microvascular endothelial complete medium with the gelatin based coating solution, according to the manufacturer's instructions. Passage 3-5 were used for experiments. Cells were maintained in a humidified environment of 5% CO_2/95% air at 37°C. One day prior to irradiation, J774A.1 cells were plated at 7.6× 10^4 cells/ml in 12 well plates (CellTreat Scientific Products, LLC, Pepperell, MA, USA). For HSpMVEC, cells were cultured to 70-90% confluence in 30 mm tissue culture plates. Cells were irradiated using an RS2000 Biological Irradiator (Rad Source Technologies, Alpharetta, GA,USA) at a dose rate of 1.15 Gy/min (160 kV, 25 mA) for a total dose of 2 or 6.8 Gy as previously described [47,52]. For exposure to iron, cells were treated with a filter sterilized solution of ammonium iron III citrate (Merck, Inc., Billerica, MA, USA) and added to a final concentration of 7.0 or 12 mg/L in cell culture medium.

RNA Purification, Reverse Transcription Polymerase Chain Reaction (RT-PCR):

Spleen tissues harvested after euthanasia were immediately placed in RNALater buffer and stored according to the manufacturer's instructions (Qiagen, Germantown, MD, USA). At the time of RNA purification, tissues were homogenized with an Ultra Turrax homogenizer (Jahnke & Kunkel, Staufen, Germany). Tissue samples were then processed using QIAshredder mini columns (Qiagen). RNA was isolated from the tissue homogenate using the RNeasy mini kit (Qiagen), and genomic DNA was removed using the RNase-free DNase Set (Qiagen). For J774A.1 or HSpMVECs, media was removed and the cells were washed twice with cold PBS. Cells were lysed in RNAlater (Qiagen, Rockville, MD, USA) with β-mercaptoethanol. Total RNA was isolated from cultured cells using the RNeasy Mini Kit (Qiagen, Valencia, CA, USA) according to the manufacturer's protocol. Purified RNA was quantified spectroscopically, reverse transcribed, and used for qPCR. Details for RNA purification, reverse transcription, and qPCR are detailed in the Supplemental Section. Sequences for qPCR primers for *Mus musculus* are shown in Table 1; qPCR primers for *Homo sapiens* are given in Table 2. Relative gene expression to the housekeeping genes was calculated using the ΔΔCq method using CFX Maestro software, 2.0 (Bio-Rad) [53,54]. For quantification, the comparative threshold cycle (CT) method was performed using Microsoft Excel 13 (Microsoft, Redmond, WA, USA) to assess relative changes in mRNA levels between the untreated control and the drug- or iron-treated and/or irradiated samples.

Western blotting:

Western blots were performed as described [55]. Cells were lysed in RIPA buffer (1% NP-40, 0.1% SDS, 0.1% Na-deoxycholate, 10% glycerol, 0.137 M NaCl, 20 mM Tris pH [8.0]) (ThermoFisher Scientific, Waltham, MA, USA), with protease inhibitors (#A32953, ThermoFisher) and phosphatase inhibitors (#A32957, ThermoFisher). Spleen tissues and cells were homogenized in RIPA buffer. Proteins were resolved by

SDS-PAGE (Criterion TGX precast, Bio-Rad) and transferred to nitrocellulose membrane. Details for protein preparation and western blotting are provided in the Supplemental Section. Western blot protein bands were detected and quantified using the Odyssey system (LI-COR). Proteins were normalized to β-actin which was used to probe the same gel. Gel images were prepared using Odyssey System software and Corel Draw X7 Graphics software (Corel Corporation, Ottawa, Ontario, Canada), in accordance with the Author Guidelines. Full gels are provided in the supporting materials.

Statistical Analysis:

Statistical analysis was performed using GraphPad Prism V6 (GraphPad Prism Software, Inc., San Diego, CA, USA). Results are represented as means ± SEM. P values of < 0.05 were considered significant. Two-way ANOVA with either Tukey or Sidak post-hoc tests were used for multiple comparisons.

Declarations

Acknowledgements

We would like to thank Mr. Michael Woolbert, USUHS, Bethesda MD, USA, for assistance with the RS2000 X-ray irradiator, and the University of Wisconsin Medical Radiation Research Center, Madison, WI, USA, for assisting with TLD calibration for dosimetry. This work was supported by Award Number DM178018 (P.I. Regina M. Day) from the Defense Medical Research and Materiel Command, Radiation Health Effects Research Program, Joint Program Committee 7. Some of the authors are employees of the U.S. Government, and this work was prepared as part of their official duties. Title 17 U.S.C. §105 provides that 'Copyright protection under this title is not available for any work of the United States Government.' Title 17 U.S.C §101 defines a U.S. Government work as a work prepared by a military service member or employees of the U.S. Government as part of that person's official duties. The views in this article are those of the authors and do not necessarily reflect the views, official policy, or position of the Uniformed Services University of the Health Sciences, the Armed Forces Radiobiology Research Institute, Department of the Navy, Department of Defense, or the U.S. Federal Government.

Author contributions:

WBR – data collection, analysis, interpretation, writing; JES – data collection, analysis, interpretation, writing; JMM – data analysis, interpretation, writing; S-HL– data analysis, interpretation, writing; MR– data collection, writing; GVB– data collection, analysis, interpretation, writing; AS– study design, data interpretation, writing; RMD – study design, data collection, analysis, interpretation, writing.

Competing Interests:

All authors confirm that there are no competing financial or non-financial interest with this manuscript.

Funding:

This work was supported by Defense Medical Research and Development Program (DMRDP) grant VP000264-01 to RMD and DMRDP grant FY18.6.1-2 to AS.

References

1. Macia, I. G. M., Lucas Calduch, A. & Lopez, E. C. Radiobiology of the acute radiation syndrome. *Rep Pract Oncol Radiother.* **16**, 123-130 (2011).
2. Kennedy, A. R., Maity, A. & Sanzari, J. K. A review of radiation-induced coagulopathy and new findings to support potential prevention strategies and treatments. *Radiat Res.* **186**, 121-140 (2016).
3. Wagemaker, G. Heterogeneity of radiation sensitivity of hemopoietic stem cell subsets. *Stem cells (Dayton, Ohio).* **13 Suppl 1**, 257-260 (1995).
4. Singh, V. K., Romaine, P. L., Newman, V. L. & Seed, T. M. Medical countermeasures for unwanted CBRN exposures: part II radiological and nuclear threats with review of recent countermeasure patents. *Expert Opin Ther Pat.* **26**, 1399-1408 (2016).
5. Peslak, S. A.*et al.* Sublethal radiation injury uncovers a functional transition during erythroid maturation. *Exp Hematol.* **39**, 434-445 (2011).
6. Cheki, M., Shirazi, A., Mahmoudzadeh, A., Bazzaz, J. T. & Hosseinimehr, S. J. The radioprotective effect of metformin against cytotoxicity and genotoxicity induced by ionizing radiation in cultured human blood lymphocytes. *Mutat Res.* **809**, 24-32 (2016).
7. Puchala, M., Szweda-Lewandowska, Z. & Kiefer, J. The influence of radiation quality on radiation-induced hemolysis and hemoglobin oxidation of human erythrocytes. *J Radiat Res.* **45**, 275-279 (2004).
8. Zhang, B., Liu, B., Zhang, H. & Wang, J. Erythrocyte stiffness during morphological remodeling induced by carbon ion radiation. *PLoS One.* **9**, e112624 (2014).
9. Elliott, T. B.*et al.* Combined immunomodulator and antimicrobial therapy eliminates polymicrobial sepsis and modulates cytokine production in combined injured mice. *Int J Radiat Biol.* **91**, 690-702 (2015).
10. Zhang, X. H., Lou, Z. C., Wang, A. L., Hu, X. D. & Zhang, H. Q. Development of serum iron as a biological dosimeter in mice. *Radiat Res.* **179**, 684-689 (2013).
11. Xie, L.-H.*et al.* Mechanisms of an increased level of serum iron in gamma-irradiated mice. *Radiat Environ Biophys.* **55**, 81-88. (2016).
12. Evstatiev, R. & Gasche, C. Iron sensing and signalling. *Gut.* **61**, 933-952 (2012).
13. Winterbourn, C. C. Toxicity of iron and hydrogen peroxide: the Fenton reaction. *Toxicol Lett.* **82-83**, 969-974 (1995).

14. Valko, M., Jomova, K., Rhodes, C. J., Kuca, K. & Musilek, K. Redox- and non-redox-metal-induced formation of free radicals and their role in human disease. *Arch Toxicol.* **90**, 1-37 (2016).
15. Carocci, A., Catalano, A., Sinicropi, M. S. & Genchi, G. Oxidative stress and neurodegeneration: the involvement of iron. *Biometals.* **31**, 715-735 (2018).
16. Isidori, A.*et al.* Iron toxicity - Its effect on the bone marrow. *Blood Rev.* **32**, 473-479 (2018).
17. Andrews, N. C. Iron homeostasis: insights from genetics and animal models. *Nat Rev Genet.* **1**, 208-217 (2000).
18. Daher, R. & Karim, Z. Iron metabolism: state of the art. *Transfus Clin Biol.* **24**, 115-119 (2017).
19. Morgan, E. H. Cellular iron processing. *J Gastroenterol Hepatol.* **11**, 1027-1030 (1996).
20. Haase, V. H. Hypoxic regulation of erythropoiesis and iron metabolism. *Am J Physiol Renal Physiol.* **299**, F1-13 (2010).
21. Theurl, I.*et al.* On-demand erythrocyte disposal and iron recycling requires transient macrophages in the liver. *Nat Med.* **22**, 945-951 (2016).
22. Pivkin, I. V.*et al.* Biomechanics of red blood cells in human spleen and consequences for physiology and disease. *Proc Natl Acad Sci U S A.* **113**, 7804-7809 (2016).
23. Sukhbaatar, N. & Weichhart, T. Iron regulation: macrophages in control. *Pharmaceuticals (Basel).* **11** (2018).
24. Nairz, M., Theurl, I., Swirski, F. K. & Weiss, G. "Pumping iron"-how macrophages handle iron at the systemic, microenvironmental, and cellular levels. *Pflugers Arch.* **469**, 397-418 (2017).
25. Winn, N. C., Volk, K. M. & Hasty, A. H. Regulation of tissue iron homeostasis: the macrophage "ferrostat". *JCI Insight.* **5** (2020).
26. Zhang, X.*et al.* Ionizing radiation induces ferroptosis in granulocyte-macrophage hematopoietic progenitor cells of murine bone marrow. *Int J Radiat Biol.* 1-12 (2020).
27. Rittase, W. B.*et al.* Deposition of iron in the bone narrow of a nurine nodel of hematopoietic acute radiation syndrome. *Exp Hematol.* **84**, 54-66 (2020).
28. Zhang, J.*et al.* Lowering iron levels protects against bone loss in focally irradiated and contralateral femurs through distinct mechanisms. *Bone.* **120**, 50-60. (2019).
29. von Zur Muhlen, C.*et al.* Superparamagnetic iron oxide binding and uptake as imaged by magnetic resonance is mediated by the integrin receptor Mac-1 (CD11b/CD18): implications on imaging of atherosclerotic plaques. *Atherosclerosis.* **193**, 102-111 (2007).
30. von zur Muhlen, C.*et al.* Imaging monocytes with iron oxide nanoparticles targeted towards the monocyte integrin MAC-1 (CD11b/CD18) does not result in improved atherosclerotic plaque detection by in vivo MRI. *Contrast Media Mol Imaging.* **5**, 268-275 (2010).
31. Jung, M., Mertens, C., Tomat, E. & Brune, B. Iron as a central player and promising target in cancer progression. *Int J Mol Sci.* **20** (2019).
32. Barasch, J.*et al.* Disposal of iron by a mutant form of lipocalin 2. *Nat Commun.* **7**, 12973 (2016).

33. Srinivasan, G.*et al.* Lipocalin 2 deficiency dysregulates iron homeostasis and exacerbates endotoxin-induced sepsis. *J Immunol.* **189**, 1911-1919 (2012).
34. Philip, M., Chiu, E. Y., Hajjar, A. M. & Abkowitz, J. L. TLR Stimulation dynamically regulates heme and iron export gene expression in macrophages. *J Immunol Res.* **2016**, 4039038 (2016).
35. Bertino, F.*et al.* Heme and sensory neuropathy: insights from novel mutations in the heme exporter feline leukemia virus subgroup C receptor 1. *Pain.* **160**, 2766-2775 (2019).
36. Potor, L.*et al.* Oxidation of hemoglobin drives a proatherogenic polarization of macrophages in human atherosclerosis. *Antioxid Redox Signal.* **35**, 917-950 (2021).
37. Day, R. M.*et al.* Enhanced hematopoietic protection from radiation by the combination of genistein and captopril. *Int Immunopharmacol.* **15**, 348-356 (2013).
38. Lei, P., Bai, T. & Sun, Y. Mechanisms of ferroptosis and relations with regulated cell death: a review. *Front Physiol.* **10**, 139 (2019).
39. Lee, Y. J.*et al.* Sphingolipid signaling mediates iron toxicity. *Cell Metab.* **16**, 90-96 (2012).
40. Feng, H.*et al.* Transferrin receptor is a specific ferroptosis marker. *Cell Rep.* **30**, 3411-3423 e3417 (2020).
41. Agoro, R., Taleb, M., Quesniaux, V. F. J. & Mura, C. Cell iron status influences macrophage polarization. *PLoS One.* **13**, e0196921 (2018).
42. Corna, G.*et al.* Polarization dictates iron handling by inflammatory and alternatively activated macrophages. *Haematologica.* **95**, 1814-1822 (2010).
43. Leblond, M. M.*et al.* M2 macrophages are more resistant than M1 macrophages following radiation therapy in the context of glioblastoma. *Oncotarget.* **8**, 72597-72612 (2017).
44. Michalson, K. T.*et al.* Monocyte polarization is altered by total-body irradiation in male rhesus macaques: implications for delayed effects of acute radiation exposure. *Radiat Res.* **192**, 121-134 (2019).
45. Duru, N., Wolfson, B. & Zhou, Q. Mechanisms of the alternative activation of macrophages and non-coding RNAs in the development of radiation-induced lung fibrosis. *World J Biol Chem.* **7**, 231-239 (2016).
46. McCart, E. A.*et al.* Delayed captopril administration mitigates hematopoietic injury in a murine model of total body irradiation. *Sci Rep.* **9**, 2198 (2019).
47. Panganiban, R. A., Mungunsukh, O. & Day, R. M. X-irradiation induces ER stress, apoptosis, and senescence in pulmonary artery endothelial cells. *Int J Radiat Biol.* **89**, 656-667 (2013).
48. Davis, T. A., Mungunsukh, O., Zins, S., Day, R. M. & Landauer, M. R. Genistein induces radioprotection by hematopoietic stem cell quiescence. *Int J Radiat Biol.* **84**, 713-726 (2008).
49. Xing, L.*et al.* Amnion-derived multipotent progenitor cells increase gain of incisional breaking strength and decrease incidence and severity of acute wound failure. *J Burns Wounds.* **7**, e5 (2007).
50. Escribano, G. M. J., Torrado Duran, S. & Torrado Duran, J. J. *[Stability of an aqueous formulation of captopril at 1 mg/ml]. Farm Hosp.* **29**, 30-36 (2005).

51. Davis, T. A.*et al.* Timing of captopril administration determines radiation protection or radiation sensitization in a murine model of total body irradiation. *Exp Hematol.* **38**, 270-281 (2010).
52. Panganiban, R. A. & Day, R. M. Inhibition of IGF-1R prevents ionizing radiation-induced primary endothelial cell senescence. *PLoS One.* **8**, e78589 (2013).
53. Schmittgen, T. D. & Livak, K. J. Analyzing real-time PCR data by the comparative C(T) method. *Nat Protoc.* **3**, 1101-1108 (2008).
54. Pfaffl, M. W. A new mathematical model for relative quantification in real-time RT-PCR. *Nucleic Acids Res.* **29**, e45 (2001).
55. Theard, P. L.*et al.* Marked synergy by vertical inhibition of EGFR signaling in NSCLC spheroids shows SOS1 is a therapeutic target in EGFR-mutated cancer. *Elife.* **9** (2020).

Tables

Table 1

Murine gene primers for qPCR.

Gene	Forward Primer	Reverse Primer
Arg1	5'-GGAACTCAACGGGAGGGTAAC-3'	5'-TAGTCCTGTCTGCTTTGCTGTGAT-3'
Flvcr1	5'-GGCACAATATAAACACCGGGC-3'	5'-TCCGACTGTATAGACACCATGAC-3'
Fth1	5'-AGTGCGCCAGAACTACCAC-3'	5'-AGCCACATCATCTCGGTCAA-3'
Gapdh	5'-ATGTGTCCGTTGTGGACTTG-3'	5'-GGTCCTCAGTGTAGCCCAAG -3'
Gpx4	5'-CGCCAAAGTCCTAGGAAACG-3'	5'-AAGGTTCAGGAATGGGCTCC-3'
IL1b	5'-AGTTGACGGACCCCAAAAG-3'	5'-AGCTGGATGCTCTCATCAGG-3'
Il6	5'-CCCCAATTTCCAATGCTCTCC-3'	5'-CGCACTAGGTTTGCCGAGTA-3'
Itgam	5'-AGAACACCAAGGACCGTCTG-3'	5'-AATCCAAAGACCTGGGTGCG-3'
Lcn2	5'-GGACTACAACCAGTTCGCCA-3'	5'-CAAAGCGGGTGAAACGTTCC-3'
Nos2	5'-CTTTTTCCCGGAGATGGGGG-3'	5'-GAGCTTGGCTTGGTACAGTCT-3'
Slc11a11	5'-TCCGAGGAGCAAGAGGAGTAA-3'	5'-TCCCCTTTGCTATCACCGAC-3'
Slc40a1	5'-TTCCTCCTCTACCTTGGCCA-3'	5'-CTGCCACCACCAGTCCATAG-3'
Trf1	5'-AAGTGCATCAGCTTCCGTGA-3'	5'-AGACCACACTGGCCTTGATG-3'
Tfrc1	5'-GCTCGTGGAGACTACTTCCG-3'	5'-AGAGAGGGCATTTGCGACTC-3'

*Murine sequences for *Arg1* (arginase 1), *Flvcr1* (feline leukemia virus receptor; heme iron receptor), *Fth1* (ferritin heavy chain 1), *Gapdh* (glyceraldehyde-3-phosphate dehydrogenase), *Gpx4* (glutathione peroxidase 4), *Il1b* (interleukin 1 beta), *Il6* (interleukin-6), *Itgam* (integrin subunit alpha M), *Lcn2* (lipocalin-2; also known as neutrophil gelatinase associated lipocain or siderocalin), *Nos2* (inducible nitric oxide synthase), *Slc7a11* (solute carrier 7 member 11), *Scl40a1* (solute carrier 20 member 1, ferroportin),*Tfrc1* (transferrin receptor-1), *Trf1* (transferrin-1).

Table 2

Human gene primers for qPCR.

Gene	Forward Primer	Reverse Primer
CDKN1A	5'- GCCGAAGTCAGTTCCTTGTG -3'	5'- TCGAAGTTCCATCGCTCACG -3'
FTH1	5'- CCAGAACTACCACCAGGACTC-3'	5'- GAAGATTCGGCCACCTCGTT-3'
GAPDH	5'- AGCCACATCGCTCAGACAC-3'	5'- GCCCAATACGACCAAATCC -3'
TFRC1	5'- AGGACGCGCTAGTGTTCTTC-3'	5'- CCAGGCTGAACCGGGTATATG-3'

*Human sequences for *CDKN1A* (p21/waf1), *FTH1* (ferritin heavy chain 1), *GAPDH* (glyceraldehyde-3-phosphate dehydrogenase), and *TFRC1* (transferrin receptor-1).

Figures

Figure 1

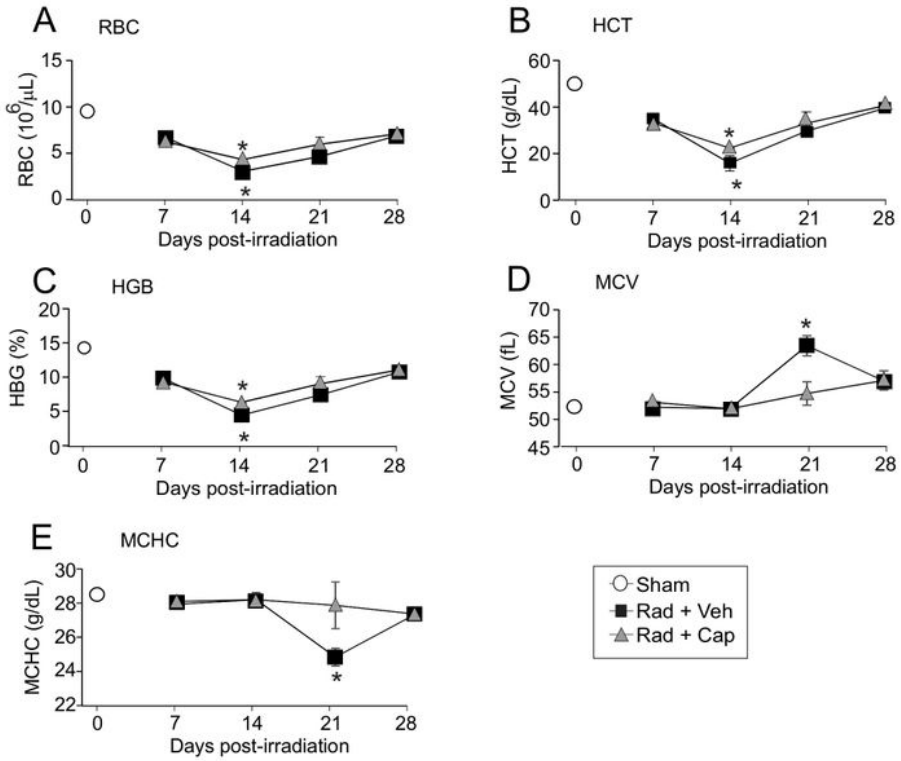

Figure 1

Total body irradiation causes decreased red blood cell, hematocrit and hemoglobin levels. C57BL/6 mice were exposed to 6.85 Gy total body irradiation. Animals received vehicle (drinking water alone) or captopril in the drinking water from days +2 - +16 post-irradiation. At the indicated time points, mice were euthanized and blood was obtained for complete blood cell counts. A. red blood cells (RBC); B. hematocrit (HCT); C. hemoglobin (HGB); D. mean corpuscular volume (MCV); and E. mean corpuscular hematocrit (MCHC). Data show means ± SEM, from n=3 animals per group; * indicates p<0.05 from control (sham irradiated) levels.

Figure 2

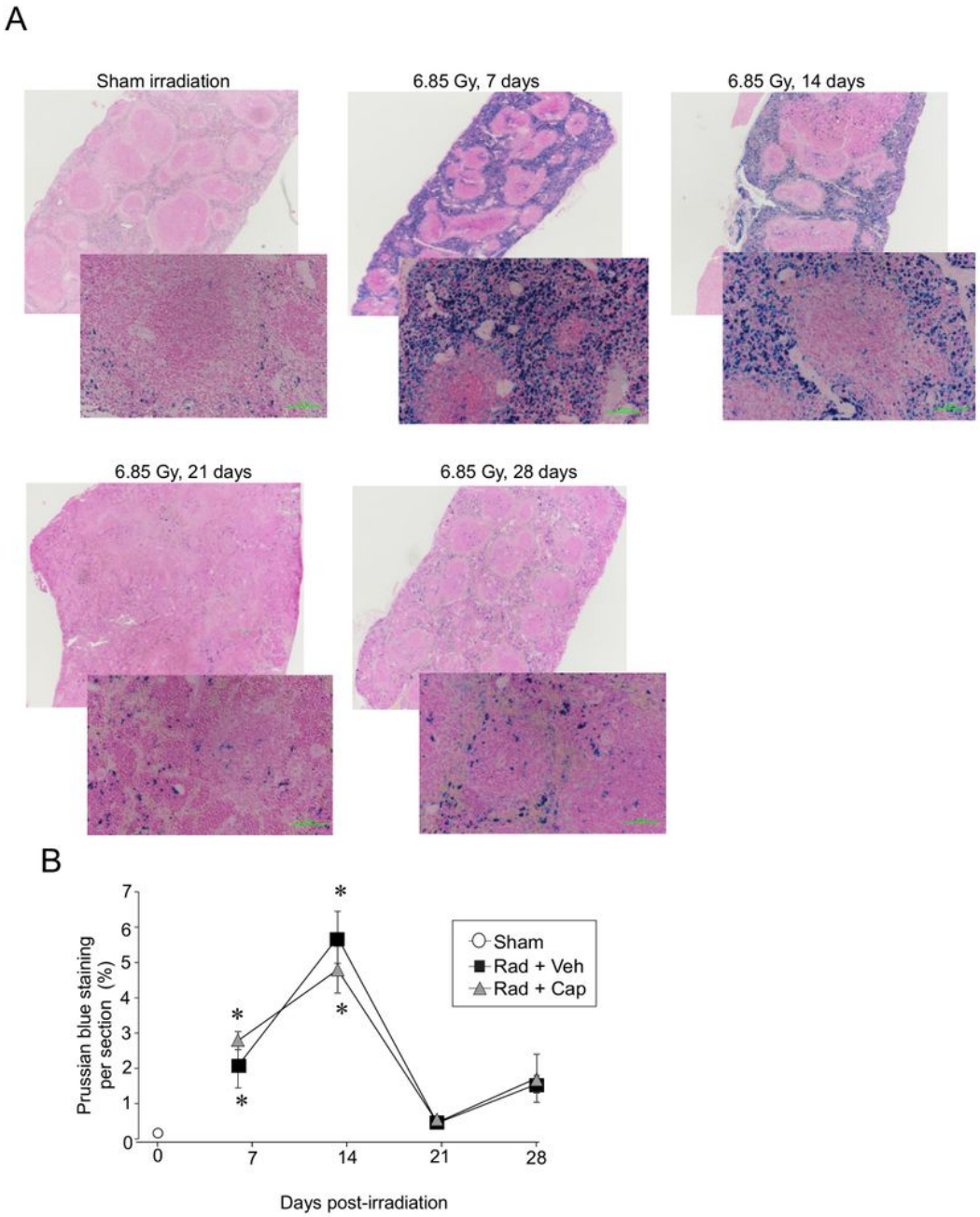

Figure 2

Total body irradiation is associated with increased Fe3+ deposition in the spleen. C57BL/6 mice were exposed to 6.85 Gy total body irradiation. Animals received vehicle (drinking water alone) or captopril in the drinking water on days +2 - +16 post-irradiation. At the indicated time points, mice were euthanized and spleen tissue was obtained for histology. A. Spleen sections were stained with Prussian blue to visualize Fe3+ content. B. Prussian blue staining was quantified. Graph shows means ± SEM from n=4 animals per group; * indicates p<0.05 from control (sham irradiated) levels.

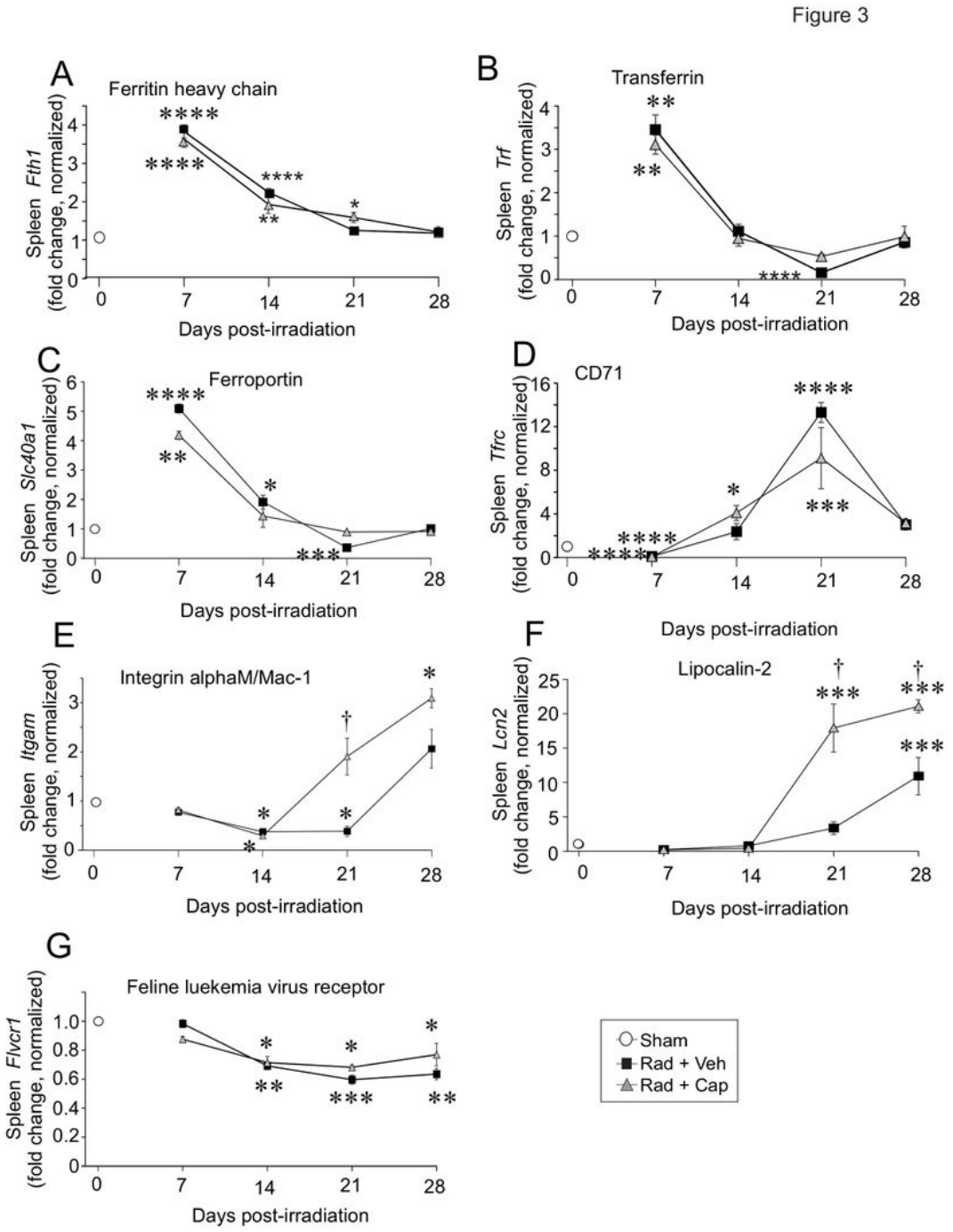

Figure 3

Total body irradiation results in increased gene expression for iron handling proteins in the spleen. C57BL/6 mice were exposed to 6.85 Gy total body irradiation. Animals received vehicle (drinking water alone) or captopril in the drinking water on days +2 - +16 post-irradiation. At the indicated time points, mice were euthanized and spleen tissue was obtained for RNA analysis. qPCR was performed for the following genes: A. Fth1 (ferritin heavy chain); B. Trf (transferrin); C. Slc40a1 (ferroportin); D. Tfrc (CD71/transferrin receptor1); E. Itgam (integrin alphaM/Mac-1); F. Lcn2 (lipocalin-2); G. Flvcr1 (feline leukemia virus receptor). Graphs shows means ± SEM from n=4 animals per group; * indicates $p<0.05$ from control (sham irradiated) levels; * indicates $p<0.05$; ** $p<0.01$; *** $p<0.001$, and **** $p<0.0001$. † indicates $p<0.05$ from vehicle-treated group at the same time point.

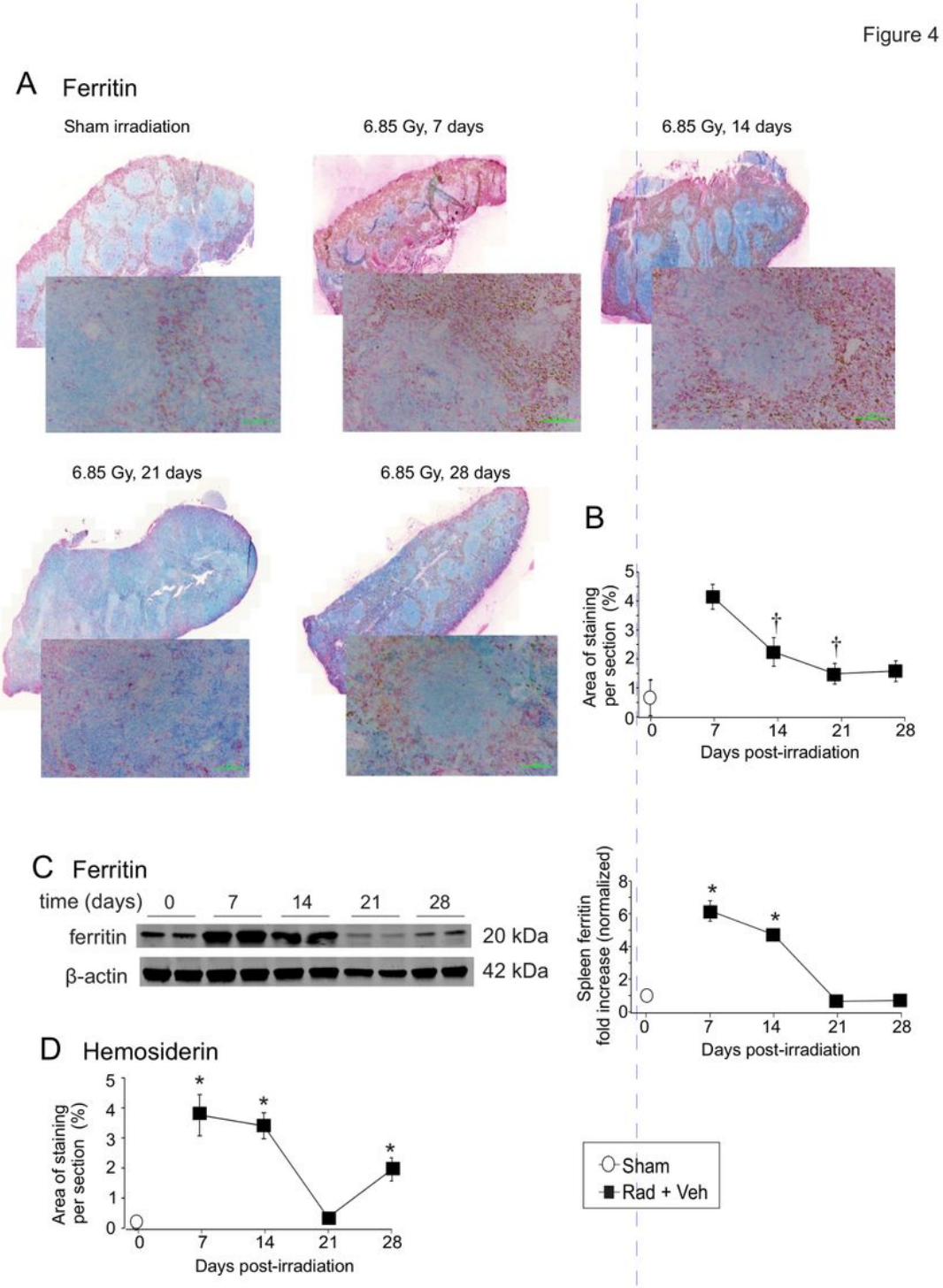

Figure 4

Total body irradiation results in increased ferritin and hemosiderin in the spleen. C57BL/6 mice were exposed to 6.85 Gy total body irradiation. At the indicated time points, mice were euthanized and spleen tissue was obtained for immunohistochemistry and western blotting. A. Spleen sections were stained for ferritin. Full spleen images were obtained with a slide scanner; insets show 30×magnification. B. Quantification of ferritin IHC staining. Graph shows means ± SEM, n=3; † indicates $p<0.05$ compared with

7 days post-irradiation. C. Western blots of ferritin in total spleen tissue; blots were reprobed for β-actin as a loading control. Representative data are shown from n=2 animals. Graph shows means ± SEM, n=4 animals; * indicates p<0.05 from control. D. Quantification of hemosiderin staining in the spleen. Graph shows means ± SEM, n=3; * indicates p<0.05 compared with control.

Figure 5

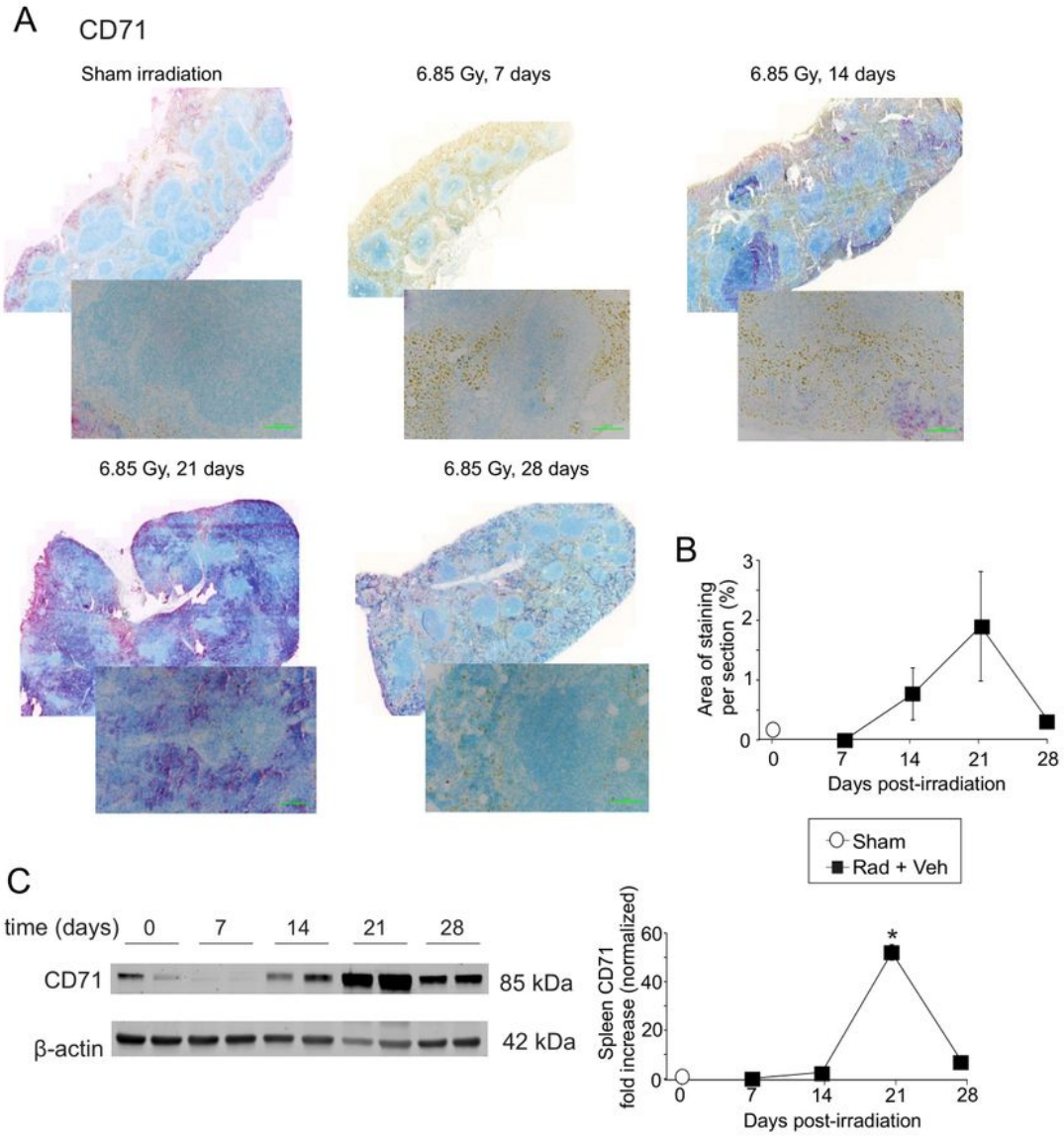

Figure 5

Total body irradiation results in increased transferrin receptor/CD71 in the spleen. C57BL/6 mice were exposed to 6.85 Gy total body irradiation. At the indicated time points, mice were euthanized and spleen tissue was obtained for immunohistochemistry and western blotting. A. Spleen sections were stained for transferrin receptor/CD71. Full spleen images were obtained with a slide scanner; insets show 30×magnification. B. Quantification of transferrin receptor/CD71 IHC staining. Graph shows means ± SEM, n=3. C. Western blots of transferrin receptor/CD71 in total spleen tissue; blots were reprobed for β-actin as a loading control. Representative data are shown from n=2 animals. Graph shows normalized means ± SEM, n=4 animals; * indicates $p<0.05$ from control.

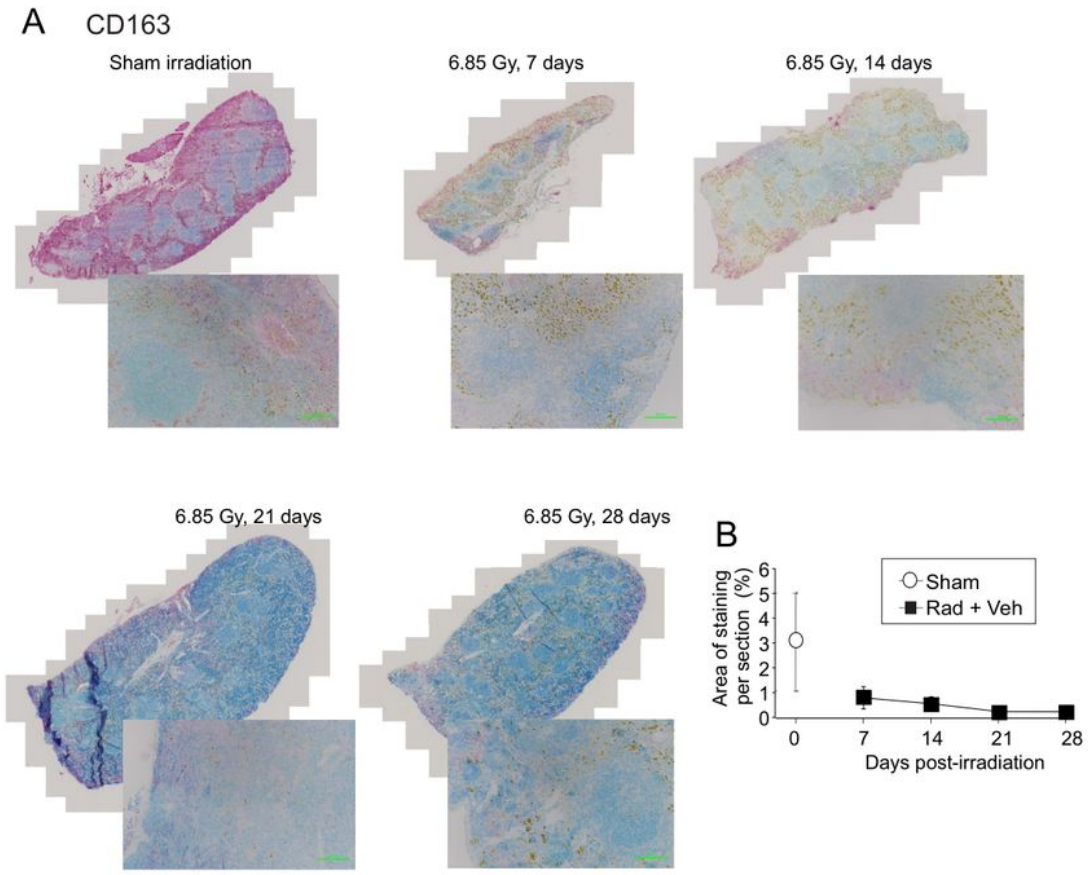

Figure 6

Total body irradiation results in a trend toward decreased CD163 in the spleen. C57BL/6 mice were exposed to 6.85 Gy total body irradiation. At the indicated time points, mice were euthanized and spleen tissue was obtained for immunohistochemistry and western blotting. A. Spleen sections were stained for CD163. Full spleen images were obtained with a slide scanner; insets show 30×magnification. B. Quantification of CD163 IHC staining. Graph shows means ± SEM, n=3.

Figure 7

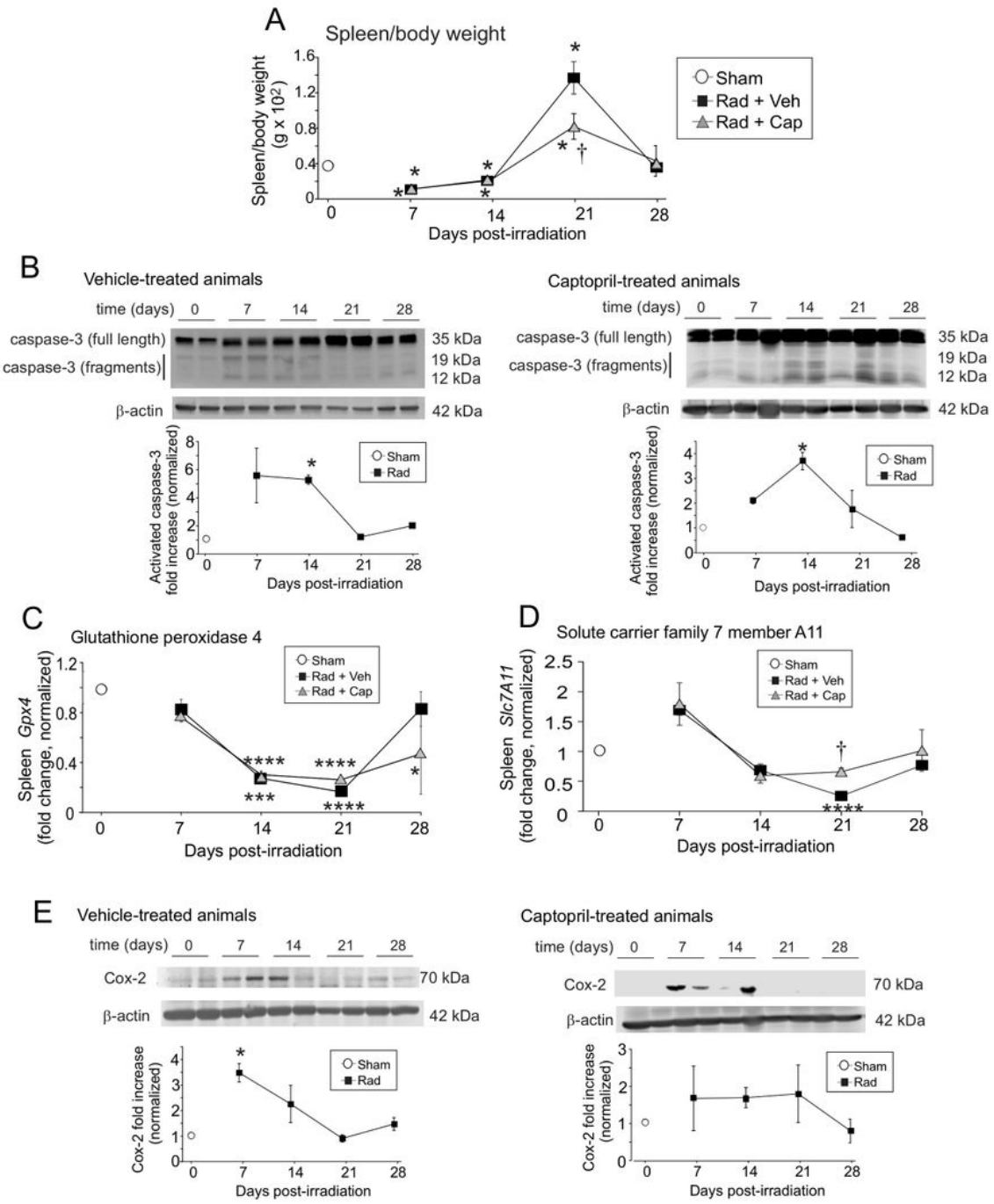

Figure 7

Total body irradiation results in biphasic alterations in spleen weight and increased expression of markers for ferroptosis in the spleen. C57BL/6 mice were exposed to 6.85 Gy total body irradiation. Animals received vehicle (drinking water alone) or captopril in the drinking water on days +2 - +16 post-irradiation. At the indicated time points, mice were euthanized and spleen tissue was obtained. Spleen weight and total body weights were obtained, and spleen tissues were used for western blotting and

qPCR. A. Spleen weights as a percentage of total body weight. Graph shows means ± SEM, n=4 animals. * indicates $p<0.05$ from control (0 time point). † indicates $p<0.05$ compared with vehicle-treated group at 21 days post-irradiation. B. Western blots of total and activated caspase 3; blots were reprobed for β-actin as a loading control. Left panel shows vehicle-treated animals; right panel shows captopril-treated animals. Representative data are shown from n=2 animals from each group. Graphs show means ± SEM, n=4 animals; * indicates $p<0.05$ from control (0 time point). C,D. Spleen tissues from sham irradiated (0 time point), vehicle-treated or captopril-treated animals was used for qPCR for glutathione peroxidase 4 (Gpx4; C) or solute carrier family 7 A 11 (Slc7a11; D). Graphs show means ± SEM, n=4 animals; * indicates $p<0.05$, *** $p<0.001$, and **** $p<0.0001$ from control (0 time point). † indicates $p<0.05$ from vehicle-treated group at the same time point. E. Western blots of COX-2; blots were reprobed for β-actin as a loading control. Left panel shows vehicle-treated animals; right panel shows captopril-treated animals. Representative data are shown from n=2 animals from each group. Graphs show means ± SEM, n=4 animals; * indicates $p<0.05$ from control (0 time point).

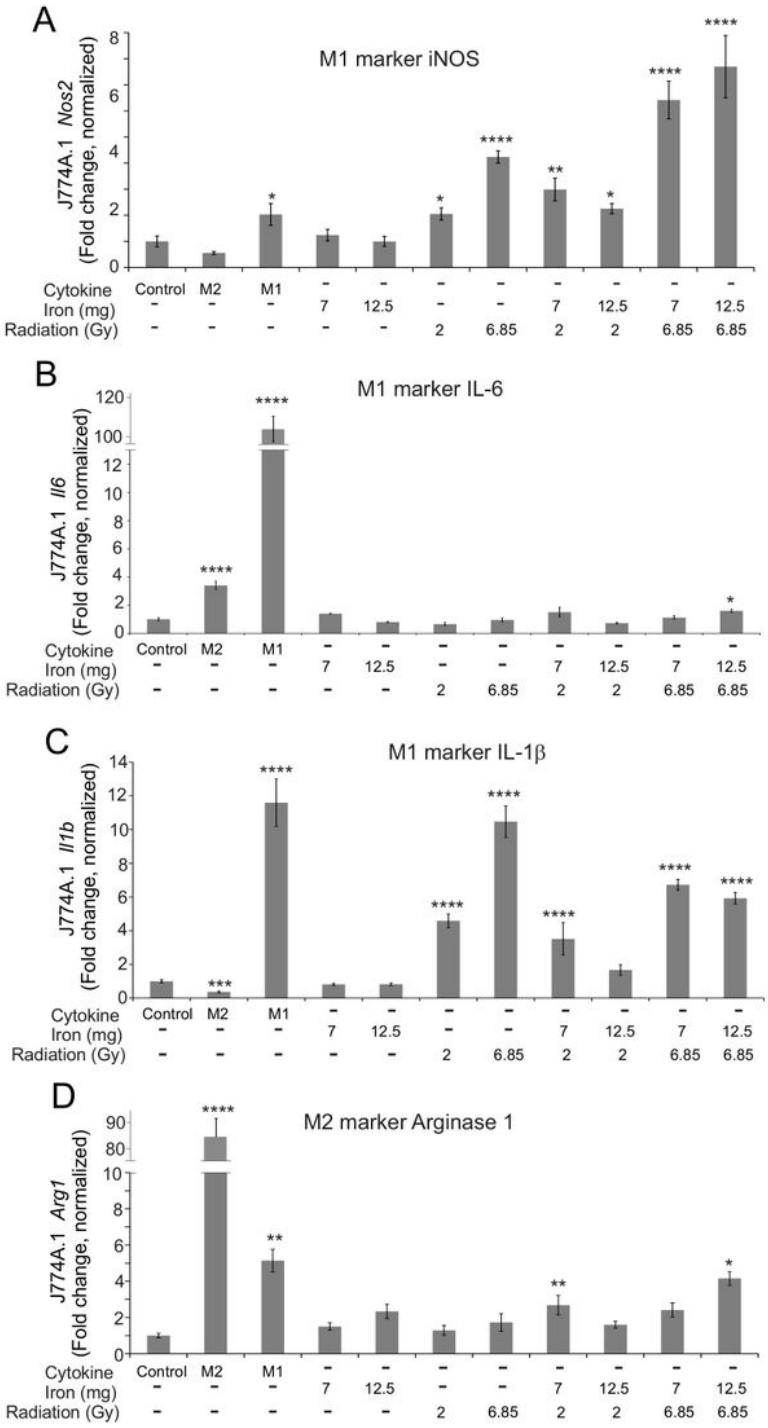

Figure 8

Effects of radiation and high iron concentrations on J774A.1 murine macrophage polarity in culture. J774A.1 cells were grown to ~80% confluence, and untreated (control) exposed to either 7 or 12 mg/L Fe3+ and/or 2 or 6.85 Gy X-ray irradiation. As a control for M2 polarization, cells were treated with 100 ng/ml IL-4; as a control for M1 polarization, cells were treated with 100 ng/ml IFN-γ + 100 ng/ml LPS. 24 h post-irradiation, RNA was purified. qPCR was performed for M1 markers (Nos2 [A], Il6 [B], and Il1b [C])

and an M2 marker (Arg1 [D]). Gene expression was normalized to Gapdh and fold increase was calculated relative to untreated cells (control). Graphs show means ± SEM, n=3 independent experiments. * indicates p<0.05, ** indicates p<0.01, **** indicates p<0.0001 compared with control.

Figure 9

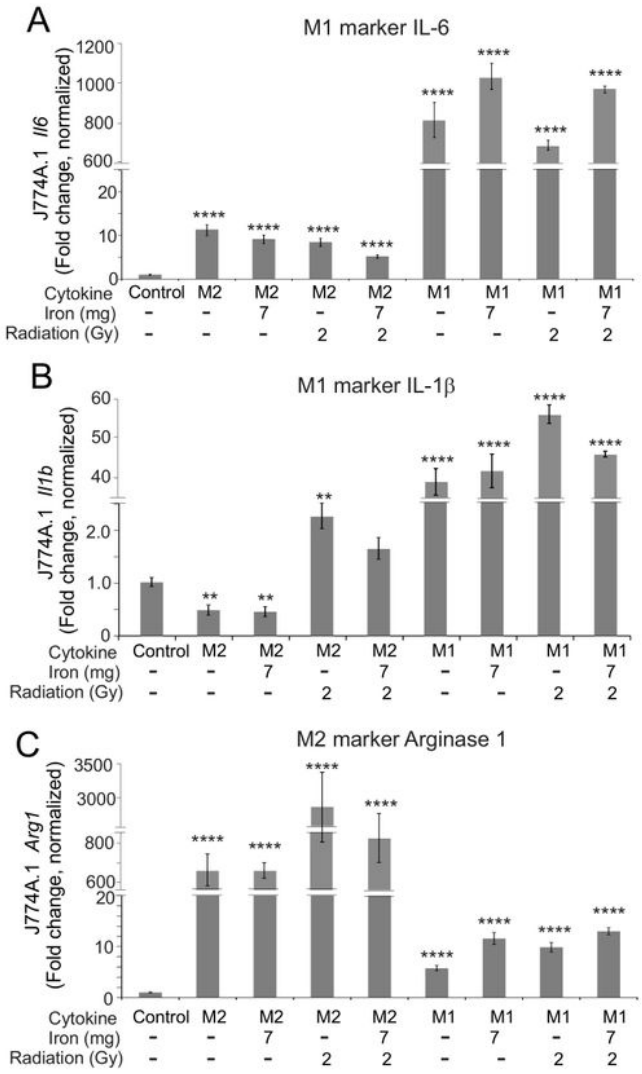

Figure 9

Effects of radiation and high iron concentrations on J774A.1 murine macrophage polarization by cytokines in culture. J774A.1 cells were grown to ~80% confluence, and untreated (control) exposed to

either 7 or 12 mg/L Fe3+ and/or 2 or 6.85 Gy X-ray irradiation. 1 h after treatments, cells were treated with 100 ng/ml IL-4 to induce M2 or 100 ng/ml IFN-γ + 100 ng/ml LPS to induce M1. As a control for M2 and M1 polarization, cells were treated with IL-4 or IFN-γ + LPS with no pretreatment. 24 h post-irradiation, RNA was purified. qPCR was performed for M1 markers (Il6 [A] and Il1b [B]), and an M2 marker (Arg1 [C]). Gene expression was normalized to Gapdh and fold increase was calculated relative to untreated cells (control). Graphs show means ± SEM, n=3 independent experiments. ** indicates p<0.01, **** indicates p<0.0001 compared with control.

Figure 10

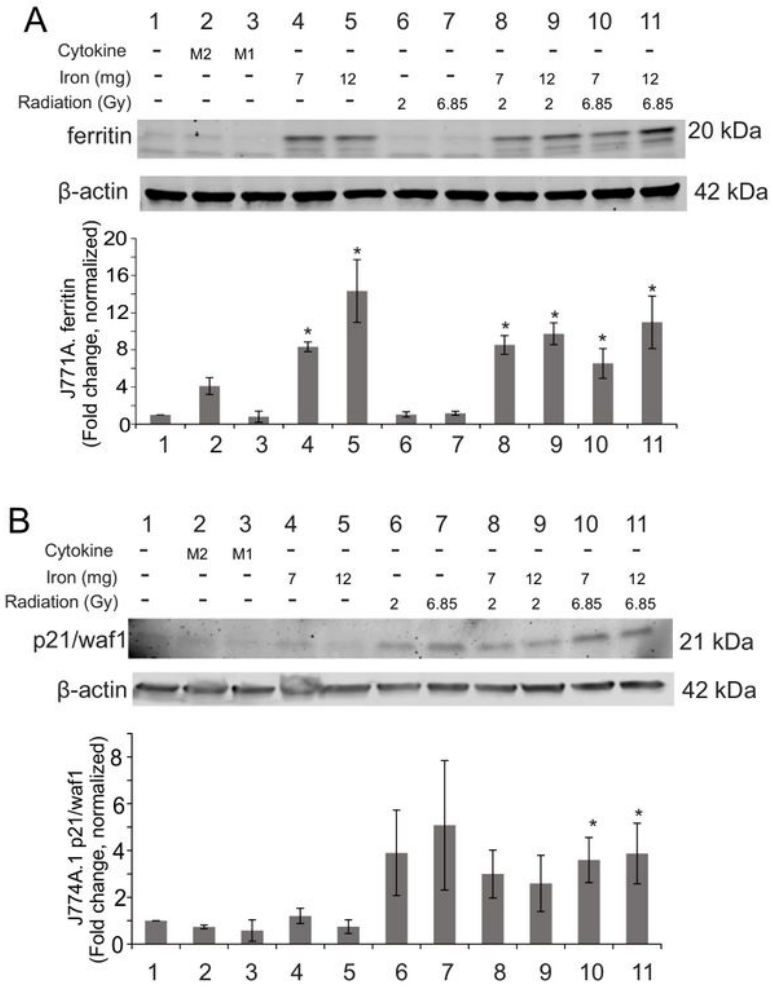

Figure 10

Effects of radiation and high iron concentrations on J774A.1 murine macrophage expression of ferritin and senescence in culture. J774A.1 cells were grown to ~80% confluence, and untreated (control) exposed to either 7 or 12 mg/L Fe3+ and/or 2 or 6.85 Gy X-ray irradiation. As a control for M2 polarization, cells were treated with 100 ng/ml IL-4; as a control for M1 polarization, cells were treated with 100 ng/ml IFN-γ + 100 ng/ml LPS. 24 h post-irradiation, Protein was purified and used for western blots for ferritin (A) or p21/waf1 (B). Blots were probed for β-actin as a loading control. Protein levels were normalized to β-actin and then the relative expression was determined compared with control levels. Graphs show means ± SEM, n=3 independent experiments. * indicaptes $p<0.05$ compared with control.

Supplementary Files

This is a list of supplementary files associated with this preprint. Click to download.

- Spleenironsuppfig1.pdf
- Spleenironsuppfig2.pdf
- Spleenironsuppfig3.pdf
- Supplementalsection.docx